18. F. Genoud, M. Guglielmi, M. Nechtschein, E. Genies, and M. Salmon, *Phys. Rev. Lett.*, **55**, (1), 118 (1985).
19. J. Tanguy and N. Mermilliod, *Synth. Met.*, To be published.
20. F. Devreux, *Synth. Met.*, To be published.
21. T. R. Jow, K. Y. Jen, R. L. Elsenbaumer, L. W. Shacklette, M. Angelopoulos, and M. P. Cava, *ibid.*, **14**, 53, 60 (1986).

The Lead Anode in Alkaline Solutions

I. The Initial Oxidation Processes

V. I. Birss* and M. T. Shevalier**

Department of Chemistry, University of Calgary, Calgary, Alberta T2N 1N4, Canada

ABSTRACT

The initial reactions occurring at a Pb anode in alkaline solutions have been investigated using cyclic voltammetry and steady-state and transient potentiostatic methodologies. It has been found that the first step in the reaction is the formation of a PbOH surface intermediate, followed by the deposition of a thin $Pb(OH)_2$ film on the Pb surface. A major portion of this film dissolves to form $Pb(OH)_3^-$ and the measured Tafel slope of 27 mV/decade of current density is consistent with the dissolution step being the rate-determining step. With the use of the rotating ring disk electrode technique, in which the disk current is separated into that due to the formation of an insoluble surface product and that due to a dissolution reaction, it was found that some of the $Pb(OH)_2$ film dehydrates to form a thin PbO film. At more positive potentials, further PbO film growth occurs, but by a nucleation and growth mechanism.

Although there is a very large body of literature concerning the electrochemical behavior of lead in acid solutions (1-5), very few papers have been concerned with the behavior of lead in alkaline solutions (6-11). The work carried out to date in alkaline solutions has utilized only steady-state approaches and has focused primarily on Pb dissolution reactions rather than on the formation of lead oxide films.

The earliest works (6, 7) were carried out using galvanostatic conditions, and it was concluded that at low applied current densities (cd), a soluble Pb^{2+} (6) or $HPbO_2^-$ (7) product was formed, while at higher cd, a PbO_2 film was thought to deposit on the Pb surface. At still higher cd, other soluble Pb species and oxygen were thought to be produced (7). However, no attempts were made to identify the film products under any of these conditions.

More recent work (8-10), also under constant cd conditions, has indicated that both PbO and PbO_2 films form on the Pb surface, with PbO hypothesized to be the primary film product (9, 10). This PbO film was also thought to be soluble, resulting in the formation of $HPbO_2^-$ in solution. The film products were identified according to the potential of their formation.

The most recent paper to appear in the literature concerning the reactions of Pb in alkaline solutions (11) involved the use of potentiostatic and potentiometric methods in order to determine the rate-determining step (rds) in the proposed reaction sequence. From the polarization curves of lead in 0.1 and 1.0*N* KOH solutions, two Tafel regions were detected, having slopes of 0.029 and 0.100V per decade of current density, at low and high cd, respectively. From these values, the following reaction scheme was proposed (11)

$$Pb + 2\,OH^- \rightleftharpoons Pb(OH)_2 + 2e^- \quad [1]$$

$$Pb(OH)_2 + OH^- \rightleftharpoons Pb(OH)_3^- \quad [2]$$

where Reaction [2] is the rds at low overpotentials and Reaction [1] is the rds at higher overpotentials. The predicted Tafel slopes of 30 and 120 mV for these two reactions are fairly close to the reported values above.

Therefore, the object of this work was to test these prior observations, primarily with the use of cyclic voltammetry (CV), potential step and rotating ring-disk electrode (RRDE) techniques, with the principal goal being to examine the mechanism and extent of Pb oxide film formation in alkaline solutions.

Thermodynamic Predictions

The potential-pH diagram for the lead-water system which appears in the Pourbaix Atlas (12) does not consider $Pb(OH)_2$ as a unique phase but rather groups it with PbO, considering it simply as hydrated PbO. In addition, the values of the free energies for some of the lead containing species in the Atlas differ from those reported more recently by the National Bureau of Standards (NBS) (13). It was for these reasons that the potential-*p*H diagram for lead was reconstructed by us, using the NBS values for the free energies and also including $Pb(OH)_2$ as a unique phase.

The theory for the construction of a potential-*p*H diagram has been given in great detail elsewhere (12). Using the potentials and the equilibrium constants calculated from the NBS free energies (13), a potential-*p*H diagram for the lead-water system was constructed and is shown in Fig. 1. Pb_2O_3 does not appear in the diagram because it is not thermodynamically stable in the presence of other species such as Pb_3O_4 and PbO_2 (12).

As can be seen from this Pourbaix diagram (Fig. 1), the electrochemistry of lead is predicted to be quite complex

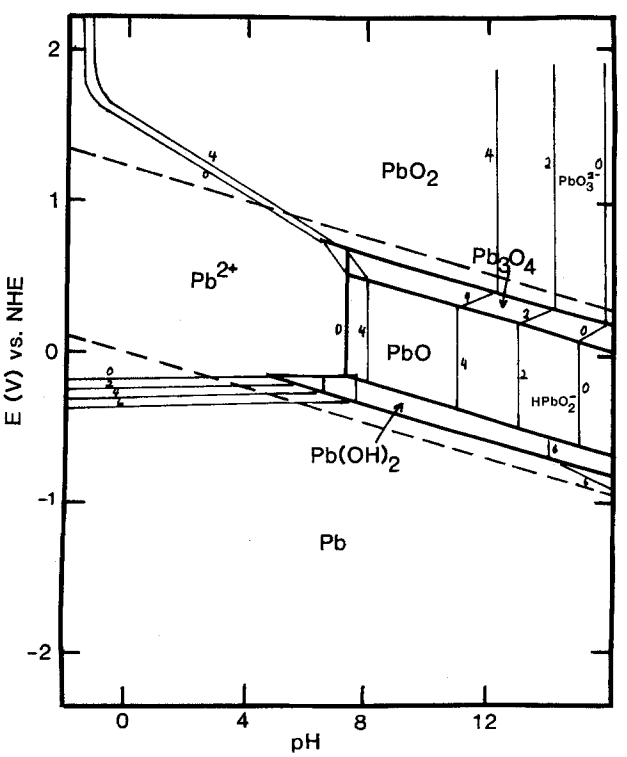

Fig. 1. Pourbaix diagram for Pb in aqueous solutions. The small numbers represent −log (concentration of soluble species).

*Electrochemical Society Active Member.
**Electrochemical Society Student Member.

in alkaline solutions, involving numerous dissolution and film forming reactions. It will be shown below that the electrochemical evidence supports this, and that numerous stable oxides and a number of dissolution reactions occur, depending primarily on the electrode potential.

Experimental

The electrochemical experiments were carried out utilizing conventional 3-electrode circuitry and a PAR 173 potentiostat coupled to a PAR 175 function generator. In the CV runs, potential sweep rates (s) were typically varied from 5 to 400 mV/s, and the resultant potential/current (E/I) curves were plotted on either a HP 7090A or a 7044 XY recorder. In potentiostatic experiments, the current/time transients (I/t) were recorded on a Nicolet 3091 digital oscilloscope, and the data was then transferred to an IBM Personal Computer.

The working electrode (WE) in the CV experiments consisted of a Pb disk (cut from a Pb rod, Johnson-Matthey Company 99.999%) press-fitted into a Teflon holder and having an exposed geometric area of 0.385 cm^2. In the potentiostatic experiments, a chip of Pb from the Pb rod was embedded in epoxy, and electrical contact was achieved with a silver wire immersed in a small pool of mercury adjacent to the Pb chip.

Before each experiment, the Pb electrode surface was treated in a reproducible manner by polishing it first with various grades of emery paper (up to 600 grit) under a stream of distilled water, then with Gamal polishing compound (Fisher) using a polishing cloth under a stream of distilled water and finally untrasonically rinsing the electrode in acetone. The electrode was then rinsed again with distilled water and electrochemically cleaned by cathodic polarization so that a steady stream of hydrogen was evolved for several minutes.

The true surface area of the WE was obtained from double layer capacitance measurements (14). A ratio of the true surface area, as determined from the double layer measurements, to the geometric surface area yields the roughness factor of the electrode. The true surface area, however, cannot be considered to be a constant in most of these experiments. For example, when a thick porous film is formed on the surface of the electrode, the surface area generally increases as the film thickens. Thus, the geometric area of the WE has been used to calculate the current density, i, when a thick porous film was formed and the "true area," as determined from the double layer measurements, was used when a thin film was formed or when essentially only Pb dissolution occurred.

The counterelectrode (CE) was a high area platinum gauze and the reference electrode (RE) was either a reversible hydrogen electrode (RHE) or a saturated calomel electrode (SCE) connected to the main cell by a Luggin capillary. In this paper, all potentials are given with respect to the RHE.

Rotating ring-disk electrode (RRDE) studies were carried out using a Pine Instruments rotator. The currents measured at the ring electrode were corrected to account for the collection efficiency, N, *i.e.*, the ratio of the amount of product which reaches the ring electrode to the amount produced at the disk electrode. N depends only on electrode geometry and is calculated using Eq. [3] (15)

$$N = 1 - f(\alpha/\beta) + \beta^{2/3}\{1 - f(\alpha)\} - (1 + \alpha + \beta)^{2/3}\{1 - f\{(\alpha/\beta)(1 + \alpha + \beta)\}\} \quad [3]$$

where

$$\alpha = (r_2/r_1)^3 - 1 \quad [4]$$

$$\beta = (r_3/r_1)^3 - (r_2/r_1)^3 \quad [5]$$

and r_1 is the radius of the disk electrode, r_2 is the inner radius of the ring, and r_3 is the outer radius of the ring electrode. $f(\phi)$, where ϕ is a general function of α and β, was calculated according to Eq. [6] (15)

$$f(\phi) = \frac{3^{1/2}}{4\pi} \ln \frac{(1 + \phi^{1/3})^3}{1 + \phi} + \frac{3}{2\pi} \arctan \frac{(2\phi^{1/2} - 1)}{(3^{1/2})} + \frac{1}{4} \quad [6]$$

The dimensions of the RRDE used in this work are r_1 = 0.250 cm, r_2 = 0.375 cm, and r_3 = 0.425 cm, yielding N = 0.2249.

The electrochemical cell utilized in this work had two compartments, one for the RE and one for the WE and the CE. The sodium hydroxide solutions were all approximately 1M in concentration and were prepared from Fisher ACS grade NaOH using thrice-distilled water. All experiments were conducted at room temperature and under room atmosphere, as preliminary experiments had shown that the electrochemical response was independent of the nature of the atmosphere.

Results and Discussion

Cyclic voltammetry.—A characteristic CV for lead in 1M NaOH at 50 mV/s is shown in Fig. 2. In this CV, there are two main anodic peaks, labeled A_1 and A_2, and two main cathodic peaks, C_1 and C_2, and O_2 and H_2 are evolved at the limits of the scan. An experiment in which the positive potential limit was increased with each complete cycle of potential showed that the anodic product formed in peak A_1 is reduced in peak C_1 and likewise for peaks A_2 and C_2. The potential obtained by extrapolating to the foot of peak A_1 is about 220 mV, which corresponds most closely to the calculated potential of 255 mV for the formation of PbO at Pb (Fig. 1). The extrapolated potential at the foot of A_2 is 1140 mV, which agrees reasonably well with the calculated potential of 1080 mV for the formation of PbO_2 from PbO (Fig. 1).

It was found that the CV of Fig. 2 could be readily reproduced between experiments and did not depend significantly on the initial electrode surface pretreatment. It was found, however, that the surface of the WE became roughened after a complete scan of potential, initially having a roughness factor of about 2, to a final roughness factor, after one complete scan, of 8. This roughening is an indication of the extent of Pb oxidation in these experiments, involving a charge density of about 500 mC/cm^2 in a complete scan of potential as in Fig. 2.

Upon closer examination of peak A_1 (Fig. 3), it can be seen that the peak is composed of two parts, a shoulder, A′, which precedes the main anodic peak and the main anodic peak itself, peak A_1. A discussion regarding the interpretation of these two anodic features will be made

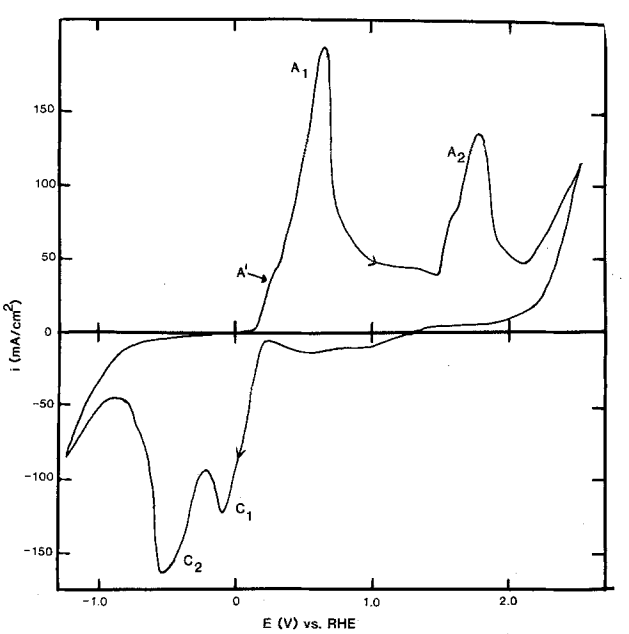

Fig. 2. A typical cyclic voltammogram for Pb in 1M NaOH; s = 50 mV/s; stationary Pb disk electrode.

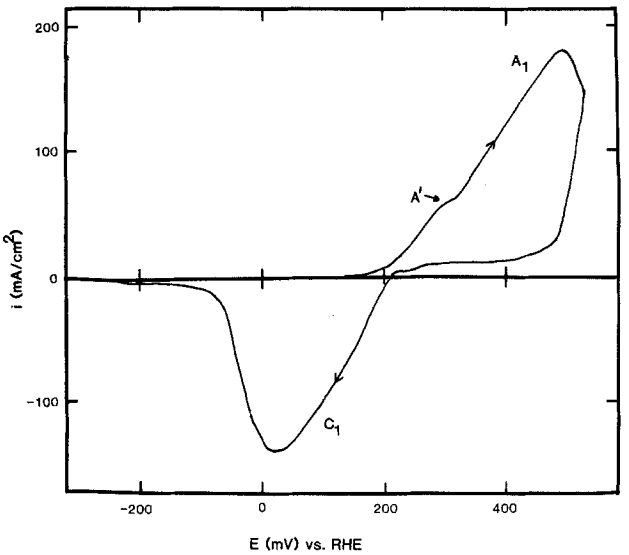

Fig. 3. Cyclic voltammogram of peak A_1 also showing shoulder, A'; s = 50 mV/s.

in an attempt to determine whether these are due to the formation of two different reaction products or are an indication of a change in the mechanism of a given sequence of reactions.

A series of CV's were obtained in the potential range primarily of shoulder A' (−300 to +300 mV) in which s was varied from 5 to 2000 mV/s. Figure 4 shows the case for s = 50 mVs^{-1}. In these experiments, the positive potential limit was increased by 10 mV in each successive cycle of potential, so that the anodic and corresponding cathodic behavior of A' could be closely observed. From this study, it was found that the initial onset of the anodic current for A' occurred at an approximate potential of 155 mV (*vs.* RHE). This potential is defined as that at which the current initially increased above the background current due, in part, to reduction of some dissolved lead species, which flowed at potentials negative of Pb oxidation (Fig. 4a). This experimentally obtained potential is closer to the calculated reversible potential (E_r) for the transition from Pb to $Pb(OH)_2$, 115 mV, than it is to the calculated Pb/PbO potential of 255 mV.

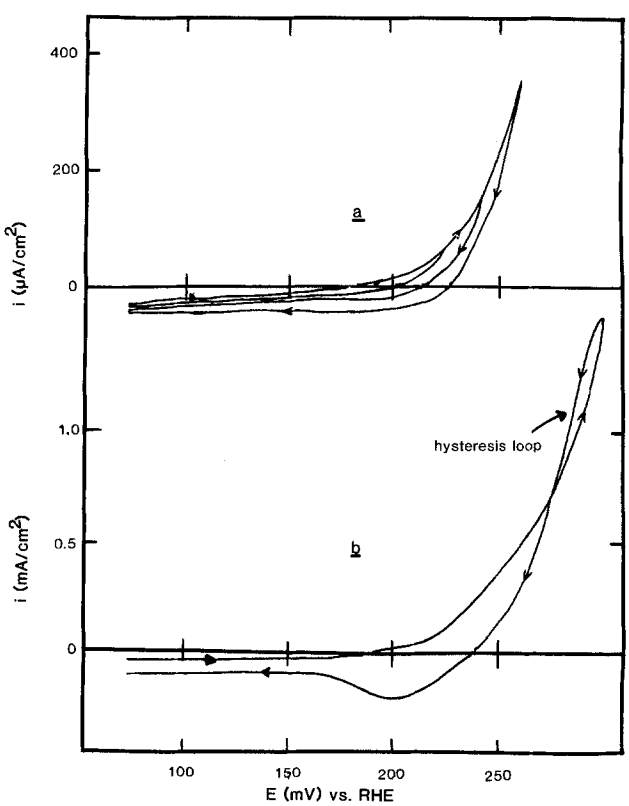

Fig. 4. Cyclic voltammograms in the region of A'. When positive limit is greater than 250 mV (b), hysteresis is observed and small cathodic peak develops; s = 50 mV/s.

As the positive potential limit was increased into A', the anodic current increased very noticeably (Fig. 4a). However, in the corresponding cathodic sweep, no cathodic current peak was observed to match the anodic shoulder, A', and therefore the anodic charge greatly exceeded the cathodic charge in this potential range. The lack of cathodic peak matching A' as well as the apparently exponentially rising anodic current (Fig. 4) appear to support the suggestion made in the prior literature (11) that an anodic dissolution reaction of Pb is the first step in the oxidation of Pb in alkaline solutions, *e.g.* Reaction [2].

When an upper potential limit exceeding 250 mV was reached, a type of hysteresis in the anodic current was observed (Fig. 4b), in which the anodic current is larger on the cathodic scan than on the preceding anodic scan. This "hysteresis loop" was found to be independent of the number of identical potential cycles the WE was subjected to. Based upon this evidence, it can be concluded that this hysteresis behavior is not due to the roughening of the WE. Instead, this type of hysteresis may be indicative of a change in the film growth mechanism, and has been observed during film nucleation processes (16). It should be noted that this hysteresis behavior is observed only when potentials at which PbO is expected to form (255 mV) are exceeded. It should also be noted that once these higher potentials are reached, a small cathodic peak can be seen (Fig. 4b), consistent with the deposition of a stable film material, *e.g.*, PbO.

In general, these results support the conclusions of previous workers. As was hypothesized by Ptitsyn *et al.* (11), the formation of $Pb(OH)_2$ in the shoulder A' may be followed by the subsequent chemical formation of the soluble $Pb(OH)_3^-$ (Reaction [2]), as seen by the lack of a cathodic peak to match the anodic shoulder. Two individual electrochemical steps are assumed to occur since it is generally accepted that a two-electron transfer reaction occurs in two consecutive one electron transfer steps (17). Following this, PbO film formation may occur via a nucleation mechanism. In order to confirm this mechanism and to distinguish the rate determining step (rds) of this film deposition/Pb dissolution reaction, potentiostatic and ring-disk electrode studies were also undertaken.

Steady-state potentiostatic method (Tafel plots).—A typical Tafel plot obtained in the potential region of shoulder A' and peak A_1 is shown in Fig. 5. The slope of this plot is 27 mV $decade^{-1}$ cd for potentials up to approximately 265 mV (*vs.* RHE) and 71 mV $decade^{-1}$ cd for potentials above this. The value of those slopes was found to be independent of electrode rotation. The presence of the higher slope indicates that either there is a change in the rds of a single reaction sequence or that a different reaction commences above about 265 mV. It should be recalled that the anodic hysteresis loop observed via CV occurred whenever the potential was extended positive of 270 mV. Thus the change in the Tafel slope is quite likely related to the process responsible for the hysteresis loop. It should also be recalled that PbO formation is predicted at 250 mV, and hence these observations may be related to the commencement of the formation of PbO. A detailed mechanistic analysis of the formation of thicker PbO films in these solutions will be discussed in a subsequent paper.

On the basis of a Tafel slope of 27 mV $decade^{-1}$ cd at a potential less than 250 mV and also on the CV results described above, the general reaction scheme previously proposed by Ptitsyn *et al.* (11) for the early stages of Pb oxidation in alkaline solutions is considered

$$Pb + OH^- \underset{k_{-1}}{\overset{k_1}{\rightleftharpoons}} (PbOH)_{ads} + e^- \qquad [7]$$

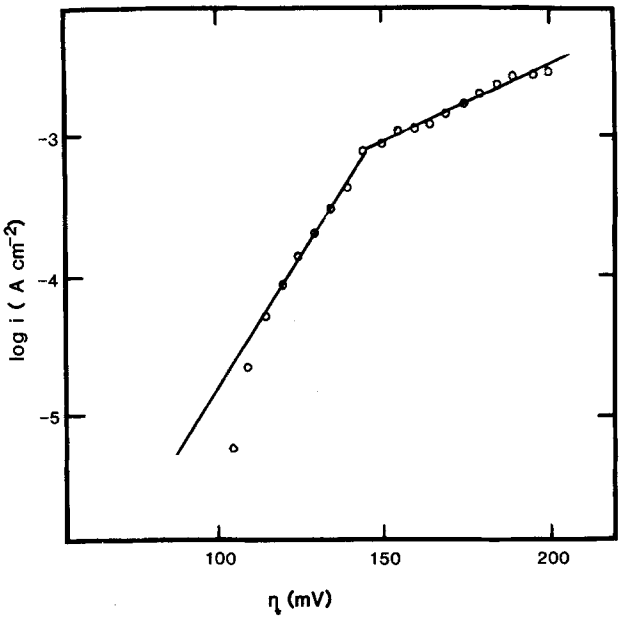

Fig. 5. Tafel plot in region of A'. Slope at lower η = 27 mV/decade cd; at higher η, 70 mV/decade cd.

$$(PbOH)_{ads} + OH^- \underset{k_{-2}}{\overset{k_2}{\rightleftharpoons}} Pb(OH)_2 + e^- \quad [8]$$

$$Pb(OH)_2 + OH^- \underset{k_{-3}}{\overset{k_3}{\rightleftharpoons}} Pb(OH)_3^- \quad [9]$$

where the k's are the rate constants of the forward and reverse reactions.

The intermediate, $(PbOH)_{ads}$, is not a known species. However, similar species have been proposed by others as intermediates in metal oxide formation, *e.g.*, a $(FeOH)_{ads}$ intermediate has been proposed in the dissolution of iron to Fe^{2+} in aqueous solutions (18, 19). Thus the postulation of a $(PbOH)_{ads}$ intermediate species is probably not unreasonable.

If the rds of this Reaction sequence (Eq. [7-9]) is considered to be Reaction [9], then the current density can be written as

$$i = \frac{\mathbf{F}k_3k_2k_1}{k_{-2}k_{-1}} (OH^-)^2 \exp\left[\frac{2\mathbf{F}\eta}{RT}\right] \quad [10]$$

so that the Tafel slope (b) is $2.3RT/2\mathbf{F}$, *i.e.*, 30 mV per decade of cd.

This is very close to the experimentally determined value of 27 mV decade^{-1}. In contrast, if Reaction [7] were the rds, the expected Tafel slope would have been 120 mV decade^{-1} cd while for [8] as the rds, the slope would be 40 mV decade^{-1} cd. These results confirm that Reaction [9] is the rds, as was reported by Ptitsyn *et al.* (11). In their work, Ptitsyn *et al.* found the Tafel slope to be 29 mV decade^{-1}. Their value of the exchange current density, i_o, was 3.0×10^{-4} A cm^{-2}, as compared to 2.6×10^{-9} A cm^{-2} found in this work (Fig. 5). However, in their Tafel plot, they have extrapolated their plot to the PbO formation potential rather than to that of $Pb(OH)_2$ deposition, as $Pb(OH)_2$ seemed to have been considered as a wet PbO species and not as a unique material. This potential is about 125 mV more positive than that for $Pb(OH)_2$ formation and accounts for the large difference in the reported i_o's.

Ptitsyn *et al.* (11) also reported a higher Tafel slope of 100 mV decade^{-1} at more positive potentials and attributed this to a change in the rds of the above reaction sequence [7-9]. They hypothesized that the rds changes from being the chemical step [9] to one of the electron transfer steps (Reaction [7]), for which a slope of 120 mV decade^{-1} cd should be obtained. This is reasonably close to the 100 mV decade^{-1} cd which they obtained experimentally.

From the present study, in which a 71 mV Tafel slope is obtained, it seems more probable that the change in the observed Tafel slope is related primarily to a change in the reaction product, *i.e.*, the formation of PbO. This is hypothesized because the change in slope occurs at a potential (265 mV) very close to the potential required for Pb to be oxidized to PbO (255 mV) and also as at approximately this potential, the current hysteresis behavior is first observed (Fig. 4), probably indicative of the onset of a new film growth mechanism. It is of interest that a 30 mV Tafel slope is also observed in the initial oxidation stages of Pb in H_2SO_4 solutions (5), consistent with a dissolution mechanism. In $HClO_4$ solutions, both a 40 mV (5) and a 30 mV slope (20) have been reported.

In the case of Cd oxidation in KOH solutions, the initial step is also thought to be Cd dissolution, as either $Cd(OH)_3^-$ or $Cd(OH)_4^{2-}$ (21). However, no evidence for the deposition of either a $Cd(OH)_2$ of CdO film during the dissolution stage was reported and a Cd oxide film was presumed to form on a surface only at more positive potentials, *i.e.*, in the region of the peak in a CV experiment (21).

Similarly, the oxidation of Zn in alkaline solutions appears to involve two one-electron transfer steps forming a Zn^{2+} species, with the second electron transfer step being rate determining (22) and leading to a 40 mV Tafel slope.

Transient potentiostatic studies.—Transient potentiostatic experiments were conducted in the region of $Pb(OH)_2$ deposition and dissolution (shoulder A') in order to test the results obtained in the steady-state potentiostatic study above.

In this work, the voltage was stepped from an initial value of 0 V (*vs.* RHE) to the final voltage in the range of A', held there for 2s and then stepped back to 0 V, with the digital oscilloscope recording the current every millisecond. A typical current transient for these experiments is shown in Fig. 6. When the final voltage was in the 27 mV/decade cd Tafel slope region, the current decreased very quickly from its initial value to a steady-state value, with both the initial and the steady-state currents being potential dependent.

The initial rapid decrease in the current was originally thought to be due only to double layer charging, but calculations showed that with a double layer capacitance of 29 μF cm^{-2} (23), the double layer charging process would be expected to be complete in approximately 40 μs while the observed decay time was well over 500 ms.

The shape of the i/t transient in Fig. 6 is consistent with the case of the random deposition of a monolayer of film, for which the cd decreases continuously with time to zero due to a decrease in the free electrode area (24). The current transient for random deposition is also potential dependent, *i.e.*, the larger the applied potential, the larger the cd (24), as was observed experimentally here. Thus, the mechanism that appears to explain the decay behavior of the experimentally obtained transient involves the random deposition of $Pb(OH)_2$ on a Pb substrate. A mechanism which had involved the nucleation

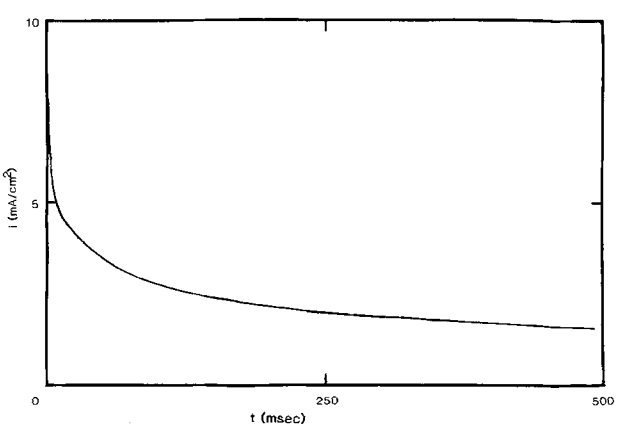

Fig. 6. i/t response to E = 0.21V *vs.* RHE

and growth of a monolayer of film would have given rise to a transient curve in which an initial rise in current is followed by a maximum (peak) and then a decline in the current. As a peak is not observed, a nucleation mechanism is rejected in this case.

The random deposition process, however, explains only the initial part of the observed current transient. Instead of the current falling to zero, as predicted in (24), the experimentally obtained cd appears to approach a limiting cd. It should be recalled that $Pb(OH)_2$ can chemically react with OH^- (Reactions [7-9]) to form a soluble $Pb(OH)_3^-$ product which can then diffuse away from the surface. This then leaves a free Pb surface which is available to electrochemically form more $Pb(OH)_2$. Thus, the steady-state cd represents the establishment of an equilibrium between the electrochemically produced $Pb(OH)_2$ and the chemically formed $Pb(OH)_3^-$.

Figure 7 shows a schematic composite of these two *i/t* responses to a potential pulse in the region of shoulder A′. Initially, the random deposition of a two-dimensional layer of $Pb(OH)_2$ occurs (Reactions [7] and [8]) causing the initial decay behavior. At longer times, Reaction [9] contributes, leading to a steady-state anodic dissolution reaction. Therefore, the results can be said to support the suggested mechanism (Reactions [7-9]) elucidated from the steady-state measurements above.

Rotating ring-disk electrode experiments.—A RRDE study of the anodic shoulder region was undertaken in an effort to distinguish separately the $Pb(OH)_2$ film deposition reaction from the concurrent dissolution process (Reactions [8] and [9]). The RRDE is an excellent technique for such a study since soluble products formed at the disk can be monitored at the ring while the insoluble products remain at the disk. The current measured at the ring (i_{ring}) is then first corrected to account for the collection efficiency (N) and is then subtracted from the current measured at the disk, i_{disk}. The resultant current, i_{film}, represents that due to surface reactions involving insoluble products

$$i_{film} = i_{disk} - N(i_{ring}) \quad [11]$$

It is of interest to note that in the case of Cd dissolution in alkaline solutions, i_{disk} could be fully accounted for by i_{ring}, supporting the contention that a Cd oxide film is not stable during Cd dissolution (21). However, in this study with Pb, it will be shown that a stable Pb oxide film can be detected by this method.

Both i_{disk} and i_{ring} are shown in Fig. 8 for the case where the disk potential was cycled between 0 and 300 mV and the ring potential was held at 0 V. This latter potential is significantly more negative than that required to form PbO, $Pb(OH)_2$ or the soluble species $Pb(OH)_3^-$ and $HPbO_2^-$ at a Pb electrode, and hence all of these species would be reducible at the ring at this potential. Therefore, by monitoring i_{disk} and i_{ring} as a function of the changing disk potential, Eq. [11] can be utilized to separate the observed current at the disk into components due to the formation of both soluble and insoluble products.

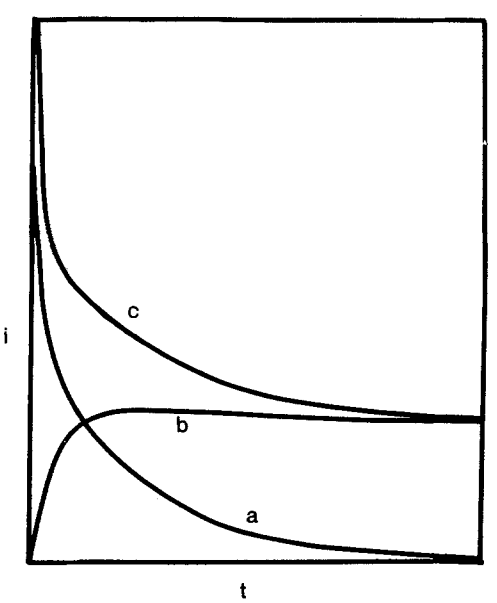

Fig. 7. Schematic of *i/t* response anticipated for random deposition of two-dimensional $Pb(OH)_2$ film (curve a), dissolution of $Pb(OH)_2$ (curve b), and sum of curves (a) and (b) (curve c).

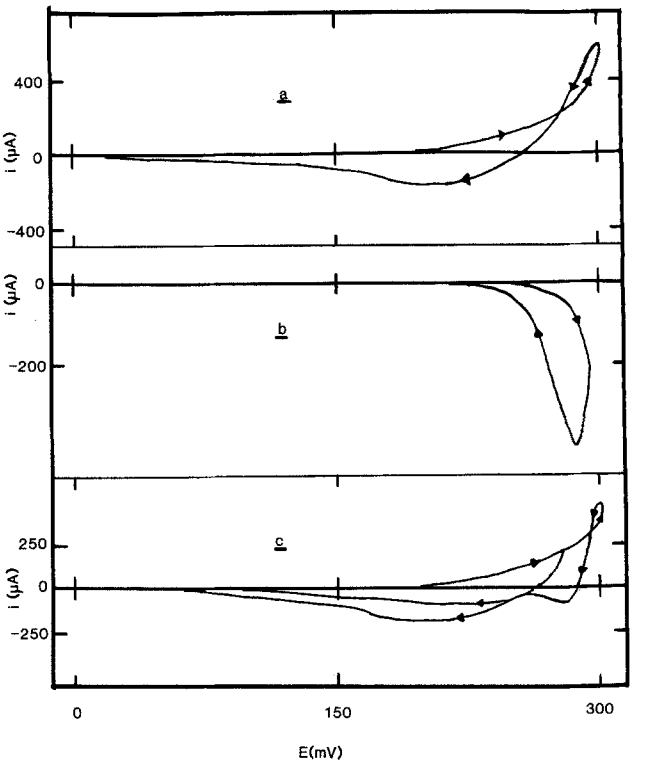

Fig. 8. Cyclic voltammograms observed using ring-disk electrode technique in region of A′; s = 20 mV/s. i_{disk} (a); i_{ring} (b); $i_{disk} - Ni_{ring}$ (c). Note the hysteresis at positive limit of (a) and (c) in region of PbO film growth.

During the forward potential sweep at the disk, i_{ring} is seen to increase (cathodically) rather slowly (Fig. 8b), indicating that some dissolution is occurring at the disk (Fig. 8a). From Eq. [11], it can be seen that under these conditions, the current at the disk electrode in the forward sweep is due primarily to a film deposition reaction (Fig. 8c). In the negative-going sweep, both the disk current and the ring current are seen to be larger than on the anodic forward sweep. At the disk, this could be explained by an increase in the surface area due to dissolution, *i.e.*, electrode roughening, or it could be indicative of nucleation and growth controlled surface film formation. At the ring, this parallel increase in current may simply indicate that the dissolution current increases proportionally to surface area, both in the case of disk electrode roughening and in the case of nucleation at the disk, which would be characterized by an increased surface area of the film deposit.

Figure 9 shows three CV's in which the disk current has been "corrected" to account for the dissolution reaction according to Eq. [11] and thus depicts the current due to film deposition at the Pb disk only. Figure 9 shows that upon sweep reversal (at E less than 300 mV but greater than about 225 mV), a cathodic peak is observed as the surface film is removed. This is an important observation since it could not be detected on the "uncorrected" CV's (Fig. 8a) because the dissolution current dominated the total measured current, particularly in the cathodic sweep. Further, it should be noted that the charges in the anodic and the cathodic curves (Fig. 9) now match closely, which confirms that i_{film} represents the current due to surface film formation processes only.

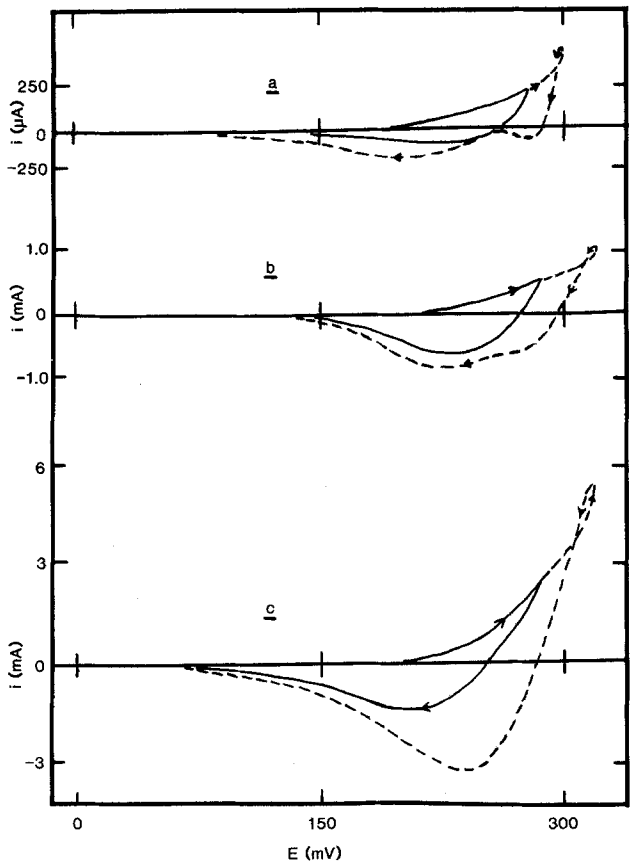

Fig. 9. $i_{disk} - Ni_{ring} = i_{film}$ in the region of A′ at s = 5 (a), 20 (b), and 50 (c) mV/s. Note that cathodic charges are very similar to anodic charges.

It was previously stated that the anodic process associated with the shoulder A′ commences at a potential of about 155 mV when monitored at the disk via CV (Fig. 4). This was compared to the calculated potentials of 115 and 255 mV for the formation of $Pb(OH)_2$ and PbO, respectively. As 155 mV is closer to the $Pb(OH)_2$ formation potential, it was assumed that A′ is associated primarily with $Pb(OH)_2$ formation on the lead substrate. The $Pb(OH)_2$ film was then thought to react with OH^- to form the soluble $Pb(OH)_3^-$ species (Reactions [7-9]). In Fig. 9, it can be seen that film deposition (probably $Pb(OH)_2$) commences at approximately 180 mV, but film reduction occurs over the potential range of 250-180 mV *vs.* RHE. This range of potential is much more positive than the calculated reversible potential of 114 mV for $Pb(OH)_2$ formation and reduction. This is a peculiar situation in that the $Pb(OH)_2$ surface deposit would be reducing at a potential well before it is thermodynamically expected to reduce.

In an effort to explain this, it is considered that the calculated reversible potential for the formation and the reduction of $Pb(OH)_2$ cannot be relied upon for the case of the formation of these thin surface films. This is because the free energy of formation of a very thin surface film may differ significantly from that of a bulk crystalline material, which is commonly used to calculate theoretical electrode potentials. If this is the case, it could still be stated that a $Pb(OH)_2$ film having somewhat different thermodynamic properties from the bulk $Pb(OH)_2$ material and hence a somewhat different potential (50-70 mV more positive) is formed and reduced in these CV's.

However, it is also possible that initially, a $Pb(OH)_2$ film is formed on the surface via Reactions [7] and [8] but that any film which does not dissolve according to [9], but remains on the surface, is rapidly dehydrated to form a PbO deposit. Both PbO and $Pb(OH)_2$ have the same oxidation state (+2) and hence an equilibrium such as is shown in Eq. [12] may exist

$$Pb(OH)_2 \rightleftharpoons PbO + H_2O \qquad [12]$$

This is consistent with the known chemical stability of PbO as compared to $Pb(OH)_2$ (16). It should be noted that if this dehydration reaction does occur, then the observed film formation potential of about 180 mV would now be negative of the calculated formation potential of 255 mV for PbO, *i.e.*, PbO is, in a sense, being underpotentially formed. This would not be unreasonable as there are numerous reports in the literature of the underpotential deposition of thin oxide films at other metals such as Pt, Au, Ir, and Ag, etc. (25-28).

If Reaction [12] is indeed occurring at the disk, then it should be added to the reaction sequence of Reactions [7]-[9]

$$Pb + OH^- \rightleftharpoons PbOH + e^- \qquad [7]$$

$$PbOH + OH^- \rightleftharpoons Pb(OH)_2 + e^- \qquad [8]$$

$$\text{parallel reactions} \begin{cases} Pb(OH)_2 + OH^- \rightleftharpoons Pb(OH)_3^- & [9] \\ Pb(OH)_2 = PbO + H_2O & [12] \end{cases}$$

In the hypothesized reaction sequence shown above, two parallel reactions are suggested, Reactions [9] and [12]. If Reaction [12] were the rds, with Reaction [9] in equilibrium, then

$$i = \frac{\mathbf{F}k_4k_2k_1}{k_{-2}k_{-1}}(OH^-)\exp\left[\frac{2\mathbf{F}\eta}{RT}\right] \qquad [13]$$

where k_4 is the rate constant for Reaction [12] and which leads to the same predicted Tafel slope of 30 mV decade^{-1} cd as when Reaction [9] was the rds. However, the reaction rate would exhibit less of a dependence on the OH^- concentration than if Reaction [9] were the rds, but this has not been tested in this work.

Conclusions

The purpose of this paper was to obtain a better understanding of the electrochemistry of lead in alkaline solution. It has been found, from a cyclic voltammetric survey, that two main anodic peaks dominate the CV, peaks A_1 and A_2, which have been shown to be related to the formation of insoluble PbO and PbO_2 films, respectively. Further, a shoulder on peak A_1 labeled as A′ has been shown to be related to the formation and reaction primarily of $Pb(OH)_2$, while these aspects of the higher Pb oxides (up to PbO_2) were not presented here.

Cyclic voltammetry has shown that shoulder A′, commencing at a potential of 155 mV, is related to the formation of $Pb(OH)_2$. However, very little $Pb(OH)_2$ remains on the Pb substrate, as shown by the lack of a matching cathodic feature to A′. This indicates that the $Pb(OH)_2$ film dissolves to form a soluble species, $Pb(OH)_3^-$. This postulated mechanism (Reactions [7]-[9]) is also supported by steady-state and transient potentiostatic results.

The steady-state potentiostatic study yielded a Tafel slope of 27 mV decade^{-1} cd, which is consistent with this reaction mechanism with Reaction [9] as the rds. The transient potentiostatic results also support this mechanism. Initially, a two-dimensional deposit of $Pb(OH)_2$ is formed on the surface of the Pb electrode by a random deposition mechanism, as seen by the rapid decay of the current transient (Fig. 6). A portion of the $Pb(OH)_2$ deposit then reacts chemically with OH^- forming the soluble $Pb(OH)_3^-$ species, leading to the observed steady-state current.

The rotating ring-disk electrode technique was used to separate the current flowing at the disk into that due to the dissolution reaction (Reaction [9]) and that due to the deposition of the stable film product, thought to be $Pb(OH)_2$ (Reaction [8]). However, the unexpectedly positive potential at which this $Pb(OH)_2$ film is reduced showed that either the reversible potential for a thin film of $Pb(OH)_2$ is different from that for bulk $Pb(OH)_2$ or that some $Pb(OH)_2$ becomes dehydrated, leaving a thin film of PbO on the Pb substrate. This chemically produced PbO would then be reducible at the observed potential.

Acknowledgments

Support of this work by the Natural Science and Engineering Council of Canada is gratefully acknowledged.

Manuscript submitted April 9, 1986; revised manuscript received Oct. 26, 1986.

REFERENCES

1. G. Archdale and J. A. Harrison, *J. Electroanal. Chem. Interfacial Electrochem.*, **47,** 93 (1973).
2. G. Archdale and J. A. Harrison, *ibid.*, **43,** 321 (1973).
3. G. Archdale and J. A. Harrison, *ibid.*, **39,** 357 (1972).
4. M. Fleischmann and H. R. Thirsk, *Trans. Faraday Soc.*, **51,** 71 (1955).
5. L. M. Baugh and K. L. Bladen, *J. Electroanal. Chem. Interfacial Electrochem.*, **145,** 325, 339, 355 (1983).
6. K. Elbs and J. Forsell, *Z. Elektrochem.*, **8,** 760 (1902).
7. S. Glasstone, *J. Chem. Soc.*, **121,** 2091 (1922).
8. P. Jones, H. R. Thirsk, and W. F. K. Wynn-Jones, *Trans. Faraday Soc.*, **52,** 1003 (1956).
9. S. S. Popova and A. V. Fortunatov, *Sov. Electrochem.*, **2,** 413 (1966).
10. S. S. Popova and A. V. Fortunatov, *ibid.*, **2,** 626 (1966).
11. M. V. Ptitsyn, G. S. Zenin, and K. I. Tikhonov, *ibid.*, **13,** 1144 (1977).
12. M. Pourbaix, "Atlas of Electrochemical Equilibria in Aqueous Solutions," 2nd ed., pp. 485-492, N.A.C.E., Houston, TX (1974).
13. D. D. Wagman, W. H. Evans, V. B. Parker, I. Halow, S. M. Bailey, and R. H. Schumm, *United States NBS Technical Note*, **270-3,** 187 (1968).
14. M. Babai, T. Tshernikovski, and E. Gileadi, *This Journal*, **119,** 1018 (1972).
15. W. J. Albery and S. Bruckenstein, *Trans. Faraday Soc.*, **62,** 1920 (1966).
16. V. I. Birss and G. A. Wright, *Electrochim. Acta*, **27,** 1429 (1982).
17. J. O'M. Bockris and A. K. N. Reddy, "Modern Electrochemistry," p. 1082, Plenum Press, New York (1977).
18. J. O'M. Bockris and A. K. N. Reddy, "Modern Electrochemistry," pp. 1080-1092, Plenum Press, New York (1977).
19. J. O'M. Bockris, D. Drazic, and A. R. Despic, *Electrochim. Acta*, **4,** 325 (1961).
20. A. S. Gioda, M. C. Giordano, and V. A. Macagno, *This Journal*, **124,** 1324 (1977).
21. R. D. Armstrong and G. D. West, *J. Electroanal. Chem. Interfacial Electrochem.*, **30,** 385 (1971).
22. R. D. Armstrong and M. F. Bell, *ibid.*, **55,** 211 (1974).
23. L. Nikolowa, *Electrochim. Acta*, **27,** 1741 (1982).
24. H. Angerstein-Kozlowska, B. E. Conway, and J. Klinger, *J. Electroanal. Chem. Interfacial Electrochem.*, **87,** 321 (1978).
25. B. E. Conway and H. Angerstein-Kozlowska, *Acc. Chem. Res.*, **14,** 49 (1981).
26. M. Fleischmann, D. J. Lax, and H. R. Thirsk, *Trans. Faraday Soc.*, **64,** 3128 (1968).
27. M. Fleischmann, D. J. Lax, and H. R. Thirsk, *ibid.*, **64,** 3137 (1968).
28. B. E. Conway, H. Angerstein-Kozlowska, B. Barnett, and J. Mozota, *J. Electroanal. Chem. Interfacial Electrochem.*, **100,** 417 (1979).

The Anodization of Heated Aluminum

C. Crevecoeur and H. J. de Wit

Philips Research Laboratories, 5600 JA Eindhoven, The Netherlands

ABSTRACT

The anodization of aluminum covered with a thin crystalline thermal oxide layer in a solution of ammoniumpentaborate in water requires less charge than the anodization of a specimen not covered with thermal oxide to the same voltage. This behavior is connected with the formation during anodization of crystalline oxide in addition to the amount initially present and with the formation of oxygen bubbles inside the anodic oxide layer. The crystalline oxide can withstand a higher electric field than the amorphous oxide. This property is used in electrolytic capacitors.

The use of crystalline aluminum oxide as a dielectric for electrolytic capacitors is important because it can sustain a higher voltage than amorphous oxide films (1). Since the dielectric constant of films containing crystalline oxide is perhaps even higher than the dielectric constant of amorphous oxide layers (2), it is in principle possible to use thinner oxide layers at a given voltage.

Anodic oxide films containing crystalline oxide can be obtained in a number of ways. An appropriate anodizing electrolyte at high temperature will lead to the formation of crystalline oxide. The protective oxide or hydroxide layers on the aluminum metal produced by heating the foil in air or by boiling it in water, respectively, are also important for the anodization process. These layers not only prevent the metal from dissolving during anodization when certain electrolytes are used (aqueous solutions of citric or adipic acid for instance) but also may cause the growth of crystalline or amorphous oxide.

In this study the formation of crystalline oxide during the anodization of flat Al samples was initiated by a thin crystalline oxide layer obtained by heating the aluminum metal in air.

The rate of oxidation is dependent on the purity of the metal (3). A number of experiments were carried out on aluminum samples containing 0.1% of magnesium, because with these samples the anodization can take place up to high voltages in the presence of a thermal oxide layer. This made it possible to determine the thickness of the crystalline and amorphous oxide layers by means of electron microscopy of thin cross sections of the anodic oxide layers.

It was found that the presence of the crystalline oxide leads to a side reaction in which oxygen gas is produced. We will show that the formation of crystalline oxide in the anodic oxide layers coincides with an apparent increased rate of anodization which is mainly due to oxygen development inside the barrier layer. Before giving more details, a short description of the thermal oxidation of Al metal will be given.

The Thermal Oxidation of Aluminum

The oxidation of aluminum above 400°C takes places in three stages: growth of amorphous oxide, a period in which crystalline oxide is formed, and a period in which the oxidation becomes extremely slow (8).

In the initial state the amorphous oxide layer on top of the metal becomes thicker, giving rise to a fast but decreasing rate of weight gain (9). The second period starts with the growth of crystals and cannot be observed below about 400°-450°C. The crystalline oxide is not obtained by crystallization of amorphous oxide but by oxygen diffusion through the thin amorphous layer covering the aluminum metal (10-12). It nucleates at the oxide-metal interface and grows along the surface of the metal until the crystallites impinge (11) or the buildup of strain in the growing crystals terminates further growth (13). The formation of the crystals at the metal-oxide interface has no effect on the growth of the amorphous layer. This layer has the same thickness on top of the alumina crystals as it has between the crystals and so the crystalline